Control of active front-end rectifier of the solid-state transformer with improved dynamic performance during precharging

Dehghani Tafti, Hossein; Cao, Shuyu; Ravi Kishore, Kanamarlapudi Venkata; Farivar, Ghias; Yeo, Howe Li; Sriram, Vaisambhayana Brihadeeswara; Pou, Josep; Tripathi, Anshuman

2017

Dehghani Tafti, H., Cao, S., Ravi Kishore, K. V., Farivar, G., Yeo, H. L., Sriram, V. B., et al. (2017). Control of active front-end rectifier of the solid-state transformer with improved dynamic performance during precharging. 2017 Asian Conference on Energy, Power and Transportation Electrification (ACEPT 2017).

https://hdl.handle.net/10356/87061

https://doi.org/10.1109/ACEPT.2017.8168622

Control of Active Front-End Rectifier of the Solid-State Transformer with Improved Dynamic Performance during Precharging

Hossein Dehghani Tafti[(1)], Cao Shuyu[(2)], K. V. Ravi Kishore[(2)], Ghias Farivar[(2)], Howe Li Yeo[(2)], V. B. Sriram[(2)], Josep Pou[(1)(2)], Anshuman Tripathi[(2)]
[(1)]School of Electrical and Electronic Engineering, Nanyang Technological University, Singapore.
[(2)]Energy Research Institute@NTU, Nanyang Technological University, Singapore.
email: hossein002@e.ntu.edu.sg

***Abstract*—The control of the active front-end rectifier of the three-stage solid-state transformer (SST) system is addressed in this paper. A comprehensive precharging sequence is introduced for the active front-end rectifier of the SST to limit the inrush current during the start-up process to its nominal current. The proposed precharging algorithm consists of two phases, passive and active precharging. The precharging resistor limits the current during the passive precharging, while a ramp increase of the voltage reference is used in the controller during the active precharging to prevent large inrush currents. Additionally, a feedforward voltage compensator is added to the voltage reference of the controller to improve the dynamic response at the beginning of the active precharging. The proposed algorithm is detailed and simulation results on a 4-kW active front-end converter are presented to validate its performance. The simulation results under various operation conditions show the ability of the proposed algorithm to limit the converter current to its nominal value during the precharging as well as to control the dc-link voltage under different load changes.**

***Index Terms*—Active front-end converter, grid-connected rectifier, precharging sequence, single-phase neutral-point-clamped converter, Solid-state transformer.**

I. Introduction

Solid-state transformer (SST) was initially introduced by Mc-Murray in 1970 [1] and has attracted a lot of interest in the last five decades [2], [3]. In the recent years more attention was focused on the prototype topology [4]–[6] and the basic control algorithms [7]. However, the reality is still challenging in achieving a low-cost, high-efficiency and long-life SST topology, which can be comparable with the conventional line-frequency transformers [8]. Several SST topologies have been investigated in the literature. Single-stage SST topology with ac switches in the input and output is investigated in [9], [10], while the two-stage topology with an ac-dc converter followed by an inverter is proposed in [2], [11]. The three-stage SST topology consists of an ac-dc, dc-dc (including isolation) and dc-ac inverter [12], [13], as depicted in Fig. 1. In this topology, the ac-dc converter, referred as active front-end converter in this paper, is used to rectify the grid ac voltage to the dc voltage on the medium-voltage-side (MV-side) dc-link capacitor. Afterwards, a dc-dc converter with an isolation transformer (dual active bridge converter) transfers

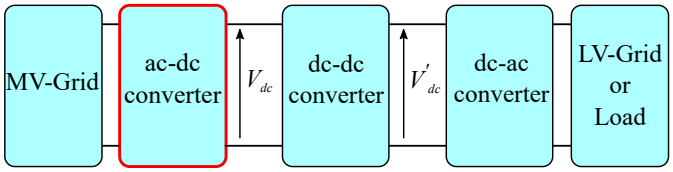

Fig. 1. Block diagram of three-stage solid-state transformer.

the power from the MV-side dc-link capacitor to the low-voltage-side (LV-side) dc-link capacitor. Finally, the dc-ac inverter converts the dc power from the LV-side dc-link to a suitable ac power for the load or low-voltage grid. The SST converter has a bidirectional power flow structure and is also able to transfer the power from the LV-grid to the MV-grid. Based on several studies [8], [14], it is concluded that the three-stage SST topology shows the best performance and controllability, compared to the single- and two-stage topologies. Hence, the three-stage SST topology is considered in this paper.

Various power converter topologies and control algorithms are available in the literature for the active front-end converter of the SST. A three-phase three-level neutral-point-clamped (NPC) converter is considered in [15]–[17] as the front-end converter, in which the dc-link voltage and current are controlled through PI controllers in the dq-frame. At the beginning of the SST operation, the voltages of the MV-side dc-link capacitors are zero, As a result, the direct connection of the converter to the grid results in large inrush currents, which can trigger the protection system or damage the power converter components. However, a comprehensive precharging algorithm, which ensures that the transient currents are limited to the converter nominal current, is not addressed in the literature [2], [3], [9]–[17].

Motivated by the above, this paper introduces a comprehensive precharging sequence for the single-phase active front-end converter of the SST, which limits the inrush current at the beginning of its operation to its nominal value. The proposed precharging algorithms consists of passive and active precharging modes. A precharging resistor is used to limit

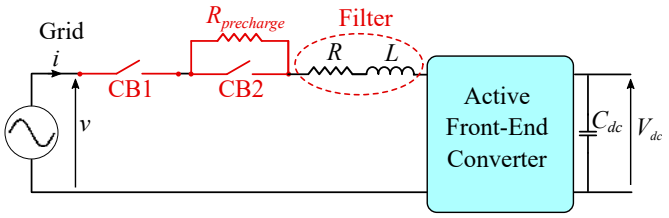

Fig. 2. Circuit configuration for the active front-end converter.

the converter current during the passive precharging, while a linear-ramp voltage reference is applied in the controller to limit the current during the active precharging. Additionally, a feedforward voltage compensator is added to the calculated voltage reference to prevent from large inrush currents at the beginning of the active precharging stage. A fictive-axis-emulator is implemented in the controller to calculate the β-axis current, based on the α-axis voltage, filter inductance and resistance. The performance of the proposed control algorithm is simulated on a 4-kW single-phase three-level NPC active front-end converter under various operating conditions and results are presented.

The rest of the paper is organized as follows. Section II provides an overview of the active front-end converter circuit configuration. The detailed implementation of the proposed algorithms for capacitor precharging as well as the normal operation of the converter are explained in Section III. Simulation results of a 4-kW grid-connected three-level neutral-pint-clamped active front-end converter are provided in Section IV, while the conclusions of the work are summarized in Section V.

II. Circuit Configuration

The circuit configuration of the active front-end converter is illustrated in Fig. 2. The converter is connected to the grid through a filter inductor (L), which reduces the injected current harmonics to the grid in order to comply with grid standards [18], [19]. The resistance of the filter and connection wires is modeled as R. The dc-link capacitor of the converter is connected to the load, which can be passive or active. Different types of converters can be used as the active front-end converter, including two-level or a multilevel single-phase converters. The proposed precharging sequence and control strategy are general algorithms and can be implemented for different types of grid-connected single-phase converters.

The circuit breaker CB1 is used for the connection/disconnection of the converter from the grid. During faults, the protection system disconnects the converter from the grid by switching off CB1. The precharging resistor ($R_{precharge}$) is used for the precharging of dc-link capacitors at the beginning of the operation of the converter. The circuit breaker CB2 bypasses the precharging resistor during the normal operation of the converter. The details of the proposed operation sequence for precharging the dc-link capacitors are explained in the following sections.

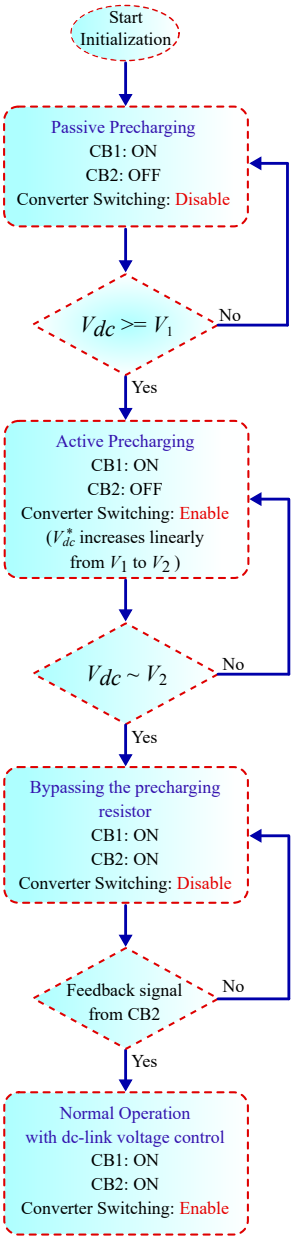

Fig. 3. Proposed capacitor precharging sequence for the active front-end converter of the solid-state transformer.

III. Proposed Control Strategy

The operation of the active front-end converter consists of two operation modes: 1) Precharging the dc-link capacitors at the beginning of the operation and 2) normal operation of the converter with controlling the dc-link voltage. At the beginning of the SST operation, the proposed precharging sequence is implemented and afterwards the converter starts its normal operation.

A. Proposed Precharging Sequence

The proposed capacitor precharging sequence is depicted in Fig. 3. Before the start of the operation, the circuit breaker CB1 is off. At the beginning of the precharging sequence, CB1

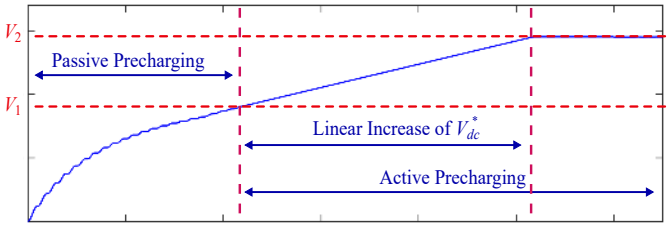

Fig. 4. dc-link voltage reference profile during the precharging sequence.

becomes on to connect the SST system to the MV-grid. During this period, the circuit breaker CB2 is off. Therefore, the current (i) flows through the precharging resistor ($R_{precharge}$). The converter switching is also disabled all of the IGBT switches are off. The converter operates similar to a passive diode rectifier and hence, this operation mode is named as passive precharging. The resistor $R_{precharge}$ is designed based on the grid peak voltage, dc-lick capacitor size and the nominal peak current of the IGBT switches. As a result, the maximum transient current at the beginning of the operation is limited to the converter nominal current.

The passive precharging can increase the dc-link voltage (V_{dc}) up to the grid peak voltage. However, the nominal value of V_{dc} is always designed to be larger than the grid peak voltage to achieve sufficient range of the modulation index for the converter. Therefore, it is not possible to increase the dc-link voltage to its nominal reference value through the passive precharging. Consequently, an active precharging is necessary to increase the dc-link voltage to its nominal reference value. A threshold voltage value of V_1 is set for the dc-link voltage, in which the operation mode changes from the passive precharging to active precharging mode, as depicted in Fig. 4.

During the active precharging mode, the controller and converter switchings are enabled, while CB2 is kept off in order to ensure that the converter current is limited to its nominal value. Additionally, in order to avoid a fast step response of the controller, the voltage reference of the dc-link voltage controller is set to V_1 at the beginning of the active precharging mode. Afterwards, it linearly increases from V_1 to its nominal reference value (V_2), as illustrated in Fig. 4. This linear increment of the voltage reference does not create an step error to the input of the controller and prevents from high transient currents during this operation mode. During this active precharging period, the dc-link voltage linearly increases to its nominal value.

Once the dc-link voltage reaches its nominal value, the calculated current reference by the controller reduces approximately to zero and accordingly, the instantaneous input current of the converter becomes close to zero. As shown in Fig. 3, at this moment, the precharging resistor is bypassed by turning on the circuit breaker CB2. Since the implemented current controller is sensitive to the total amount of the system resistance, the implemented resistance value in the controller should be changed after bypassing $R_{precharge}$. Although,

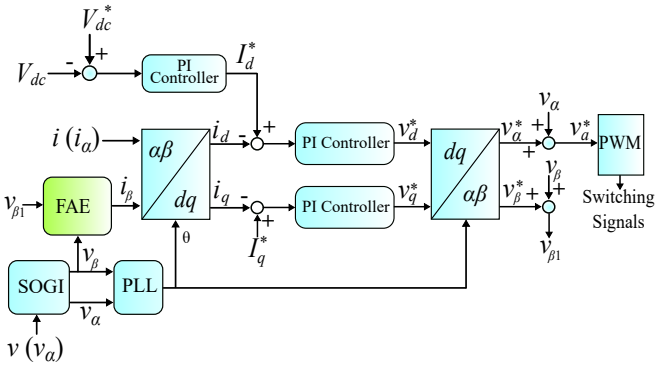

Fig. 5. Schematic of the controller for the active front-end converter of the solid-state transformer.

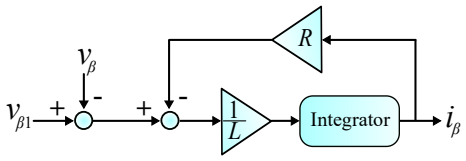

Fig. 6. Diagram of the fictive-axis emulator.

the exact connection time of CB2 can not be determined. Therefore, the controller and switching of the converter is disabled. This operation mode prevents a large transient in the current controller, due to the mismatch between the resistor value that is applied in the controller and the real resistance of the converter system. The converter stays at this operation mode until the circuit breaker CB2 sends a connection feedback signal from. After receiving a connection feedback, the controller and converter switching are enabled and the converter starts its normal operation by controlling the dc-link voltage. The detailed implementation of the controller during the normal operation is presented in the following subsection.

B. Control Strategy During Normal Operation

The schematic of the implemented control strategy for the operation of the grid-connected single-phase converter during the normal operation is illustrated in Fig. 5. Firstly, the dc-link voltage (V_{dc}) is compared with its reference value (V_{dc}^*) and the error is fed into a PI controller. The output of the PI controller is the d-axis current reference (I_d^*), which relates to the input active power of the rectifier. The input reactive power of the converter can be adjusted by setting the q-axis current reference (I_q^*). This value is set to zero in this study in order to achieve the unity power factor operation for the converter.

The calculation of the grid voltage angle is implemented by using a phase-locked-loop (PLL) controller. The detailed implementation of the PLL can be found in [20]. The implementation of the PLL requires both α- and β-axis voltages. Accordingly, a second order generalized integrator (SOGI) algorithm is applied to calculate the β-axis voltage (v_β) from v_α. A comprehensive explanation of SOGI is presented in [21].

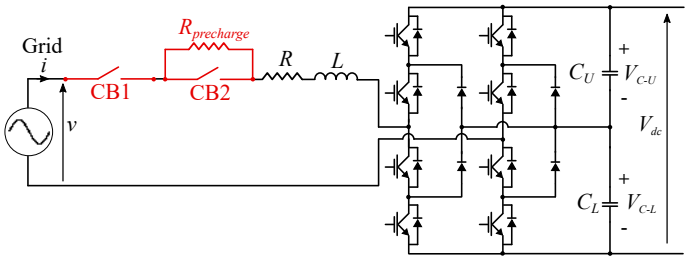

Fig. 7. Simulation verification - circuit configuration of the grid-connected single-phase three-level neutral-point-camped active front-end converter.

TABLE I
SIMULATION PARAMETERS OF THE ACTIVE FRONT-END CONVERTER

Parameter	Symbol	Value
Nominal power	P_{nom}	4 kW
Grid voltage	v	760 V_{rms}
Filter inductor	L	8 mH
Filter resistance	R	0.6 Ω
Precharging resistance	$R_{precharge}$	70 Ω
dc-link voltage	V_{dc}	1450V
dc-link capacitor	C_U / C_L	1.5mF
Switching frequency	f_{sw}	5 kHz
Voltage level to change to active precharging	V_2	900 V

The PI controller is easy for implementation compared to the proportional resonant (PR) controller and it is also more robust to grid voltage harmonics [22], [23]. Hence, the current controller is executed using the PI controller in the dq-frame. I_d^* and I_q^* are calculated from the dc-link voltage controller and grid requirement for reactive power injection, as mentioned above. The α- and β-axis currents are necessary for the calculation of instantaneous d- and q-axis currents (i_d and i_q), . The α-axis current (i_α) is equal to the measured current of the converter (i). A fictive axis emulator (FAE) is applied in this study for the calculation of the β-axis current (i_β). The diagram of the FAE is illustrated in Fig. 6 and comprehensive explanation can be found in [24].

The errors between the instantaneous dq-axis currents and their calculated reference values are fed into two PI controllers, which calculate the dq-axis voltage references (v_d^* and v_q^*). These values are transferred to $\alpha\beta$-frame using the inverse Clark transformation and the calculated voltage angle (θ) from the PLL. In order to achieve a fast response during grid voltage variations and low transient current at the beginning of the operation of the controller, a feedforward voltage compensator is applied to the calculated $\alpha\beta$-frame voltage references, as shown in Fig. 5. The feedforward compensator for α- and β-axises are v_α and v_β, respectively, which are calculated from the PLL. Finally, the voltage reference (v_a^*) is fed into the pulse-width-modulation (PWM) technique to calculate the switching signals.

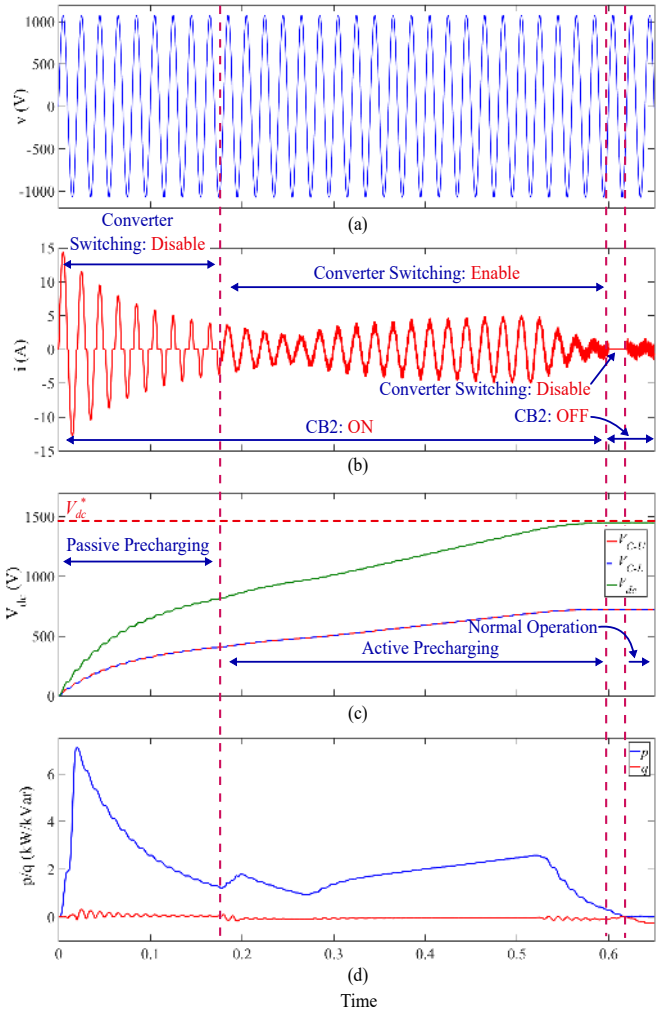

Fig. 8. Simulation results: *Case I* - performance of the proposed algorithm during the precharging of the dc-link capacitors: (a) Grid voltage, (b) grid current, (c) dc-link capacitors voltages and (d) active and reactive power of the converter.

IV. SIMULATION RESULTS

A 4-kW active front-end single-phase rectifier is modeled and developed using PLECS toolbox. A three-level neutral-point-clamped (NPC) converter is considered as the converter in this study. The circuit configuration of this system is illustrated in Fig. 7, while the main system parameters are listed in Table I. The NPC converter applies two series connected capacitors (C_U and C_L) in the dc-link. Therefore, a voltage balancing algorithm is required to ensure that the voltage of these capacitors are close to each other during all of the operation conditions. For this purpose, a voltage balancing algorithm with the modification of the voltage reference, based on the implemented algorithm in [25], is applied in this study. Three case studies are considered for the evaluation of the performance of the proposed algorithms: *Case I*: Precharging operation, *Case II*: ramp reduction of the load power and *Case III*: step increase of the load power.

Case I: The performance of the proposed precharging sequence is evaluated in this case study and results are

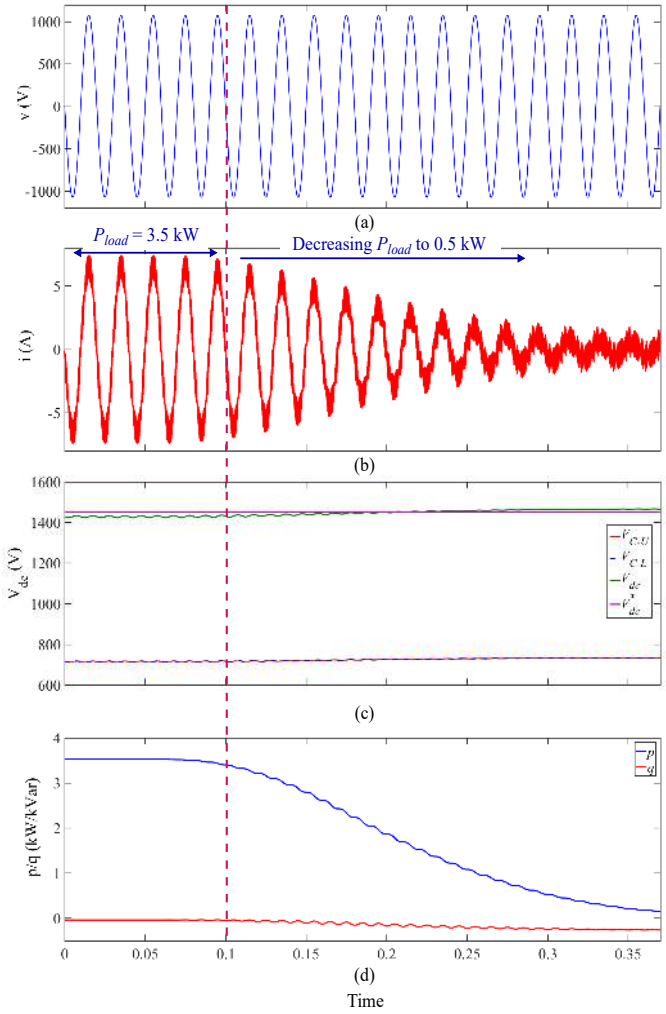

Fig. 9. Simulation results: *Case II* - performance of the proposed algorithm under the ramp decrease of the load power: (a) Grid voltage, (b) grid current, (c) dc-link capacitors voltages and (d) active and reactive power of the converter.

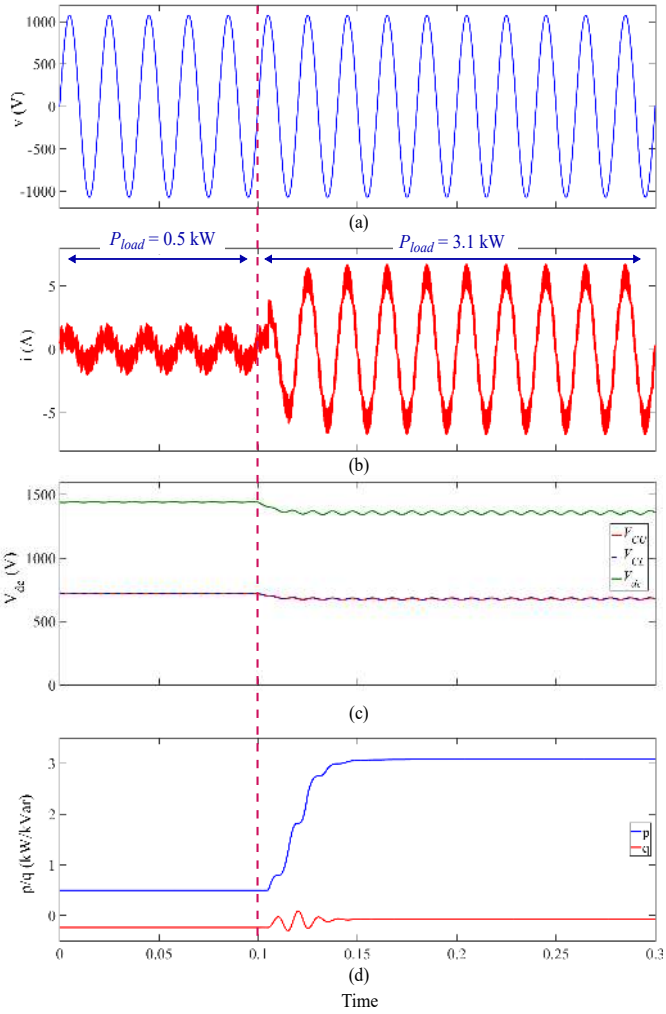

Fig. 10. Simulation results: *Case III* - performance of the proposed algorithm under the step increase of the load power: (a) Grid voltage, (b) grid current, (c) dc-link capacitors voltages and (d) active and reactive power of the converter.

illustrated in Fig. 8. At the beginning, the voltages of the dc-link capacitors are zero, as presented in Fig. 8(c). The passive precharging increases the dc-link voltage to 900 V within a period of 0.18 s. During this period, the current flows through $R_{precharge}$ and its maximum value at the first cycle is smaller than 15 A, which is within the nominal current range of the rectifier. The current waveform, shown in Fig. 8(b), is similar to the current waveform of a passive diode converter. It also can be observed that by increasing of V_{dc}, the maximum value of the injected current is reduced.

At $t = 0.18$ s, the dc-link voltage reaches the voltage value V_1, which is set in the controller and hence the operation mode of the converter changes to the active precharging by enabling the switching signals of the NPC converter. There is no high transient current at the starting of the active precharging, due to the feedforward compensation added to the controller, as presented in Fig. 5. Additionally, V_{dc}^* linearly increase from 900 V to 1450 V in a period of 0.4 s. As a result the converter current increases linearly in order to regulate the dc-link voltage to V_{dc}^*.

After reaching V_{dc} to its nominal reference value (1450 V) at $t = 0.55$ s, the converter current and power reduces close to zero, as depicted in Fig. 8(d). Afterwards, at $t = 0.6$ s the precharging resistor is bypassed and the switching of the converter is also disabled. According the current becomes zero during this period. Finally, after receiving the connection feedback from circuit breaker at $t = 0.62$ s, the converter starts its normal operation and load can be connected to the output of the converter.

Case II: The performance of the proposed control algorithm under a ramp reduction of the load is investigated in this case study and results are presented in Fig. 9. Before $t = 0.1$ s, the load power is equal to 3.5 kW and accordingly, the peak current of the rectifier is 8 A and the converter regulates V_{dc} to 1450 V. During the ramp reduction of the load power, the converter current is decreased linearly, while the implemented controller is able to regulate the dc-link voltage

at its reference value. During the reduction of the power, the phase shift between the voltage and current remains at zero; hence, the converter reactive power is zero, as shown in Fig. 9. It should be noted that due to the implementation of the voltage balancing algorithm, the dc-link capacitors are equal to each other during all of the operation conditions.

Case III: In this case study, the performance of the implemented controller under a step increase of the load from $0.5\,\mathrm{kW}$ to $3.1\,\mathrm{kW}$ is evaluated and results are depicted in Fig. 10. As a result of this load power step-change, the rectifier current increases from $1\,\mathrm{A}$ to approximately $5\,\mathrm{A}$ in less than $0.05\,\mathrm{s}$. Additionally, the dc-link voltage is regulated to its reference value, after a small decrease. The simulation results show the applicability of the implemented control algorithm in adjusting the dc-link voltage under various load change conditions. Additionally, the evaluation results during the precharging of capacitors show the capability of the proposed precharging sequence in limiting the active front-end rectifier current to its nominal value at the beginning of the operation of the SST.

V. Conclusion

A precharging sequence consists of a passive and an active precharging algorithms for the active front-end rectifier of the SST system has been proposed in this paper. A linear ramp voltage reference increment has been implemented during the active precharging to prevent from high transient currents in the rectifier. Additionally, a feedforward voltage compensator has been applied to improve the dynamic performance at he beginning of the operation and under grid voltage sags. The implementation of the proposed precharging sequence as well as the controller during the normal operation have been explained in detail. The evaluation results on a $4\text{-}\mathrm{kW}$ simulation platform have also been provided in the paper. The improved performance of the proposed algorithms in limiting the inrush current to its nominal value and regulating of the dc-link voltage to its reference value under various load changes makes it suitable for three-stage solid-state transformers.

References

[1] W. McMurray, "Power converter circuits having a high-frequency link," Patent *U.S. 3 517 300*, Jun. 23, 1970.

[2] J. E. Huber and J. W. Kolar, "Solid-state transformers: On the origins and evolution of key concepts," *IEEE Ind. Electron. Magazine*, vol. 10, no. 3, pp. 19–28, Sep. 2016.

[3] Q. Chen, N. Liu, C. Hu, L. Wang, and J. Zhang, "Autonomous energy management strategy for solid-state transformer to integrate PV-assisted EV charging station participating in ancillary service," *IEEE Trans. Ind. Inform.*, vol. 13, no. 1, pp. 258–269, Feb. 2017.

[4] D. Dujic, C. Zhao, A. Mester, J. K. Steinke, M. Weiss, S. Lewdeni-Schmid, T. Chaudhuri, and P. Stefanutti, "Power electronic traction transformer-low voltage prototype," *IEEE Trans. Power Electron.*, vol. 28, no. 12, pp. 5522–5534, Dec. 2013.

[5] H. Iman-Eini, S. Farhangi, J. L. Schanen, and J. Aime, "Design of power electronic transformer based on cascaded H-bridge multilevel converter," in *Proc. IEEE Intern. Symposium on Ind. Electron.*, Jun. 2007, pp. 877–882.

[6] H. Fan and H. Li, "High-frequency transformer isolated bidirectional DC-DC converter modules with high efficiency over wide load range for 20 kVA solid-state transformer," *IEEE Trans. Power Electron.*, vol. 26, no. 12, pp. 3599–3608, Dec. 2011.

[7] X. Yu, X. She, X. Zhou, and A. Q. Huang, "Power management for DC microgrid enabled by solid-state transformer," *IEEE Trans. Smart Grid*, vol. 5, no. 2, pp. 954–965, Mar. 2014.

[8] H. Chen and D. Divan, "Soft-switching solid state transformer (S4T)," *IEEE Trans. Power Electron.*, vol. PP, 2017.

[9] H. A. Toliyat, A. Balakrishnan, M. Amirabadi, and W. Alexander, "Soft switched ac-link AC/AC and AC/DC buck-boost converter," in *Proc. IEEE Power Electron. Specialists Conf.*, Jun. 2008, pp. 4168–4176.

[10] R. Limpaecher and E. Limpaecher, "Charge transfer apparatus and method," Patent *U.S. 9 329 596*, Sep. 12, 2000.

[11] K. Vangen, T. Melaa, and A. K. Adnanes, "Soft-switched high-frequency, high power DC/AC converter with IGBT," in *Proc. 23rd Annual IEEE Power Electron. Specialists Conf. (PESC)*, Jun. 1992, pp. 26–33.

[12] X. She, R. Burgos, G. Wang, F. Wang, and A. Q. Huang, "Review of solid state transformer in the distribution system: from components to field application," in *Proc. IEEE Energy Conversion Congress and Exposition (ECCE)*, Sep. 2012, pp. 4077–4084.

[13] D. Dujic, F. Kieferndorf, F. Canales, and U. Drofenik, "Power electronic traction transformer technology," in *Proc. IEEE 7th Intern. Power Electron. and Motion Control Conf.*, vol. 1, Jun. 2012, pp. 636–642.

[14] S. Falcones, X. Mao, and R. Ayyanar, "Topology comparison for solid state transformer implementation," in *Proc. IEEE PES General Meeting*, Jul. 2010, pp. 1–8.

[15] S. Madhusoodhanan, A. Tripathi, D. Patel, K. Mainali, A. Kadavelugu, S. Hazra, S. Bhattacharya, and K. Hatua, "Solid-state transformer and MV grid-tied applications enabled by 15 kV SiC IGBTs and 10 kV SiC MOSFETs based multilevel converters," *IEEE Trans. Ind. Appl.*, vol. 51, no. 4, pp. 3343–3360, Jul. 2015.

[16] S. Madhusoodhanan, S. Bhattacharya, and K. Hatua, "Control technique for 15 kV SiC IGBT based active front end converter of a 13.8 kV grid-tied 100 kVA transformerless intelligent power substation," in *Proc. IEEE Energy Conversion Congress and Exposition*, Sep. 2013, pp. 4697–4704.

[17] S. Madhusoodhanan, S. Bhattacharya, and K. Hatua, "A unified control scheme for harmonic elimination in the front end converter of a 13.8 kV, 100 kVA transformerless intelligent power substation grid-tied with LCL filter," in *Proc. IEEE Applied Power Electron. Conf. and Exposition (APEC)*, Mar. 2014, pp. 964–971.

[18] "IEEE standard for interconnecting distributed resources with electric power systems," *IEEE Std 1547-2003*, pp. 1–28, Jul. 2003.

[19] H. D. Tafti, A. I. Maswood, G. Konstantinou, J. Pou, and F. Blaabjerg, "A general constant power generation algorithm for photovoltaic systems," *IEEE Trans. Power Electron.*, 2017.

[20] M. Mirhosseini, J. Pou, V. G. Agelidis, E. Robles, and S. Ceballos, "A three-phase frequency-adaptive phase-locked loop for independent single-phase operation," *IEEE Trans. Power Electron.*, vol. 29, no. 12, pp. 6255–6259, Dec. 2014.

[21] F. B. M. Ciobotaru, R. Teodorescu, "A new single-phase PLL structure based on second order generalized integrator," in *Proc. IEEE 37th Power Electronics Specialists Conf. (PESC)*, Jun. 2006, pp. 1–6.

[22] H. D. Tafti, A. I. Maswood, A. Ukil, O. H. Gabriel, and L. Ziyou, "NPC photovoltaic grid-connected inverter using proportional-resonant controller," in *Proc. IEEE PES Asia-Pacific Power and Energy Engineering Conf. (APPEEC)*, 2014, pp. 1–6.

[23] H. D. Tafti, A. I. Maswood, Z. Lim, G. H. Ooi, and P. H. Raj, "Proportional-resonant controlled NPC converter for more-electric-aircraft starter-generator," in *Proc. IEEE 11th Intern. Conf. Power Electron. and Drive Systems (PEDS)*, 2015, pp. 41–46.

[24] B. Bahrani, A. Rufer, S. Kenzelmann, and L. A. C. Lopes, "Vector control of single-phase voltage-source converters based on fictive-axis emulation," *IEEE Trans. Ind. Appl.*, vol. 47, no. 2, pp. 831–840, Mar. 2011.

[25] H. D. Tafti, A. I. Maswood, G. Konstantinou, J. Pou, K. Kandasamy, Z. Lim, and G. H. Ooi, "Low-voltage ride-thorough capability of photovoltaic grid-connected neutral-point-clamped inverters with active/reactive power injection," *IET Renewable Power Generation*, vol. 11, no. 8, pp. 1182–1190, Jul. 2017.